algorithms

MDPI

Article

Impact of Iterative Bilateral Filtering on the Noise Power Spectrum of Computed Tomography Images

Choirul Anam [1,*], Ariij Naufal [1], Heri Sutanto [1], Kusworo Adi [1] and Geoff Dougherty [2]

[1] Department of Physics, Faculty of Sciences and Mathematics, Diponegoro University, Semarang 50275, Indonesia
[2] Department of Applied Physics and Medical Imaging, California State University Channel Islands, Camarillo, CA 93012, USA
* Correspondence: anam@fisika.fsm.undip.ac.id

Abstract: A bilateral filter is a non-linear denoising algorithm that can reduce noise while preserving the edges. This study explores the characteristics of a bilateral filter in changing the noise and texture within computed tomography (CT) images in an iterative implementation. We collected images of a homogeneous Neusoft phantom scanned with tube currents of 77, 154, and 231 mAs. The images for each tube current were filtered five times with a configuration of sigma space (σ_d) = 2 pixels, sigma intensity (σ_r) = noise level, and a kernel of 5 × 5 pixels. To observe the noise texture in each filter iteration, the noise power spectrum (NPS) was obtained for the five slices of each dataset and averaged to generate a stable curve. The modulation-transfer function (MTF) was also measured from the original and the filtered images. Tests on an anthropomorphic phantom image were carried out to observe their impact on clinical scenarios. Noise measurements and visual observations of edge sharpness were performed on this image. Our results showed that the bilateral filter was effective in suppressing noise at high frequencies, which is confirmed by the sloping NPS curve for different tube currents. The peak frequency was shifted from about 0.2 to about 0.1 mm^{-1} for all tube currents, and the noise magnitude was reduced by more than 50% compared to the original images. The spatial resolution does not change with the number of iterations of the filter, which is confirmed by the constant values of MTF50 and MTF10. The test results on the anthropomorphic phantom image show a similar pattern, with noise reduced by up to 60% and object edges remaining sharp.

Keywords: bilateral filter; computed tomography; noise power spectrum

Citation: Anam, C.; Naufal, A.; Sutanto, H.; Adi, K.; Dougherty, G. Impact of Iterative Bilateral Filtering on the Noise Power Spectrum of Computed Tomography Images. *Algorithms* **2022**, *15*, 374. https://doi.org/10.3390/a15100374

Academic Editors: Lucia Maddalena and Laura Antonelli

Received: 24 September 2022
Accepted: 10 October 2022
Published: 13 October 2022

1. Introduction

Despite its popular applications in medical imaging, computed tomography (CT) provides a relatively high-radiation dose for patients that can increase the probability of malignancy [1,2] in leukemia and brain cancer [1,3]. Various efforts were made to overcome this problem by following the "as low as reasonably achievable" (ALARA) principle [4]. The two areas of study that are most frequently explored include reducing patient doses as effectively as possible [5–7] and improving image quality for diagnostic purposes [8,9].

Image quality can be determined by selecting appropriate input parameters before scanning, such as tube current, tube voltage, rotation time, pitch, reconstruction type, reconstruction filter, and so on [10–12], and it can be enhanced at the post-processing stage. Radiographers or medical physicists select the pre-scanning input parameters and can perform noise reduction to get an improved image during post-scanning (i.e., after scanning the patient or phantom). Filtering the image using a noise reduction algorithm can not only suppress image noise but also allows patients to be exposed to a lower dose. However, although these filters can suppress noise, they tend to produce blurriness in the images [13]. Many linear denoising algorithms have been developed, such as the Wiener [14] and Gaussian filters [15].

Non-linear filters, such as the bilateral filter, non-local mean filter, total variation filter, and wavelet filter [16], can be used to overcome the shortcomings of linear filters. The bilateral filter uses two weights in the process, namely distance weighting (σ_d) and intensity weighting (σ_r) [17]. Its behavior in filtering images based on these weights results in less-noisy images while preserving edges [18], making it one of the most widely used noise-reducing filters [19].

There have been many studies of the various aspects of the bilateral filter, including theoretical studies [20], determination of optimal parameters [21,22], modification [23,24], and acceleration of the process [25,26]. However, to our knowledge, there are no studies characterizing the bilateral filter in the context of iterative filtering. Since bilateral filters can be iterated [27,28], it is necessary to explore the impact of iteration on noise texture, because noise texture is an important parameter of image quality [29–31]. This study does not introduce a new perspective on the bilateral filter, but rather it investigated the effects of iteration on bilateral filtering of CT images and analyzed its impact on the noise texture. The study aims to provide a better understanding of the nature of bilateral filters and preferences for implementing them in CT images.

2. Materials and Methods

2.1. Phantom Images

We scanned a Neusoft CT phantom (Neusoft Medical System, Shenyang, China) with the parameters shown in Table 1. Variations in tube current were used to obtain images with various noise levels. Other parameters were set to standard values often used for quality control procedures. For filtering, 5 slices of the homogeneous water phantom body of each dataset were selected. Figure 1 shows sample images using various tube currents.

Table 1. Scan parameters.

Parameter	Value
Scanner	Neusoft NeuViz 16 Classic
Tube current (mAs)	77, 154, 231
Tube voltage (kVp)	120
Slice thickness (mm)	5
Scan option	Helical
Pitch	1.2
Convolution kernel	F20
Image reconstruction	Filtered-back projection

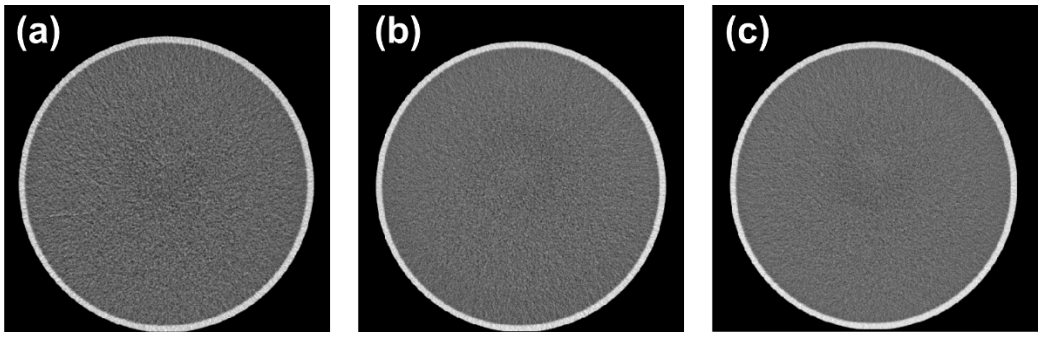

Figure 1. Sample images of a homogeneous water phantom scanned with tube currents of (**a**) 77, (**b**) 154, and (**c**) 231 mAs.

2.2. Bilateral Filter

The bilateral filter [16] uses non-linear image denoising. It was developed from the principle of spatial Gaussian convolution which is linear and only considers one weighting

factor to apply smoothing to the image. Equation (1) shows the principle of Gaussian convolution.

$$g[i,j] = \frac{1}{W_s} \sum_m \sum_n f[m,n] G_{\sigma_d}[i-m, j-n] \quad (1)$$

where g is the result of convolution, Ws is the normalization factor, f is the initial pixel value, and G is Gaussian spatial convolution. Gaussian convolution weights each pixel within the kernel according to the weighting of the Gaussian distribution evenly, so that it is still in the linear smoothing category. The bilateral filter takes this principle and adds an intensity-weighted factor. Equation (2) shows the principle of the bilateral filter.

$$g[i,j] = \frac{1}{W_{sb}} \sum_m \sum_n f[m,n] G_{\sigma_d}[i-m, j-n] G_{\sigma_r}(f[m,n] - f[i,j]) \quad (2)$$

where G_{σ_d} is a Gaussian spatial convolution and G_{σ_r} is a Gaussian intensity. In the bilateral filter, the Gaussian spatial convolution is biased with its intensity weighting taken from the neighboring pixels inside the kernel. This consideration gives a non-linear nature that produces an image with reduced noise, while still preserving the edges [27,32].

2.3. Implementation of Bilateral Filter, Measurement of Noise Power Spectrum and Spatial Resolution

The noise power spectrum (NPS) describes the texture of noise in the frequency domain [29]. The 2D NPS is estimated as shown in Equation (3) [33].

$$NPS_{(u,v)} = \frac{d_x d_y}{N_x N_y} . |\mathcal{F}[I(x,y) - P(x,y)]|^2 \quad (3)$$

where u and v are spatial frequency in the x and y direction, d_x and d_y are pixel size in mm, N_x and N_y are number of pixels in the x and y direction of the region of interest (ROI), $\mathcal{F}$ denotes the 2D Fourier transform, $I(x, y)$ is the pixel value in Hounsfield Units (HU), and $P(x, y)$ is the second order polynomial fit of $I(x, y)$.

The description of NPS is Summarized as the peak frequency (f_P) and the average frequency (f_A) shown in Equations (4) and (5) [34].

$$f_P = \arg max[NPS(f)] \quad (4)$$

$$f_A = \frac{\int f \cdot NPS(f)\, df}{\int NPS(f)\, df} \quad (5)$$

where f is the radial spatial frequency, and $NPS(f)$ is the radially averaged 1D NPS.

Before filtering an image, we measured NPS using ImQuest (Duke University, Durham, NC, USA) [35] with a total ROI of 5, a size of 64 pixels, and a sampling angle of 10. This was carried out to obtain a description of the noise in the original image before filtering. The ROIs for measuring NPS is shown in Figure 2.

The edge of the modulation transfer function (MTF) [36] was also measured automatically by IndoQCT [37] to get a more complete picture of the spatial resolution of the filtered image. The edge MTF was chosen as the spatial resolution parameter because the phantom used was a homogeneous phantom [36]. The steps to obtain the edge MTF are shown in Figure 3. A square ROI is placed on the edge of the phantom at the 12 o'clock position (Figure 3a) and then the pixels were averaged in the x-axis direction to obtain a curve called the edge spread function (ESF) (Figure 3b). Tail replacement is performed on this curve to obtain the corrected ESF shape (Figure 3c). The corrected ESF curve is then differentiated to produce a line spread function (LSF) curve (Figure 3d) which is then zeroed and normalized. The Fourier transform of the LSF curve gives the MTF curve (Figure 3e). Bilateral filtering, NPS and MTF measurements were performed sequentially on 5 selected images of a homogeneous phantom.

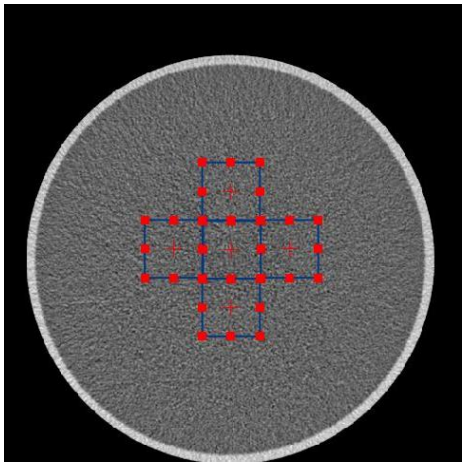

Figure 2. NPS measurement using 5 regions of interest (ROIs).

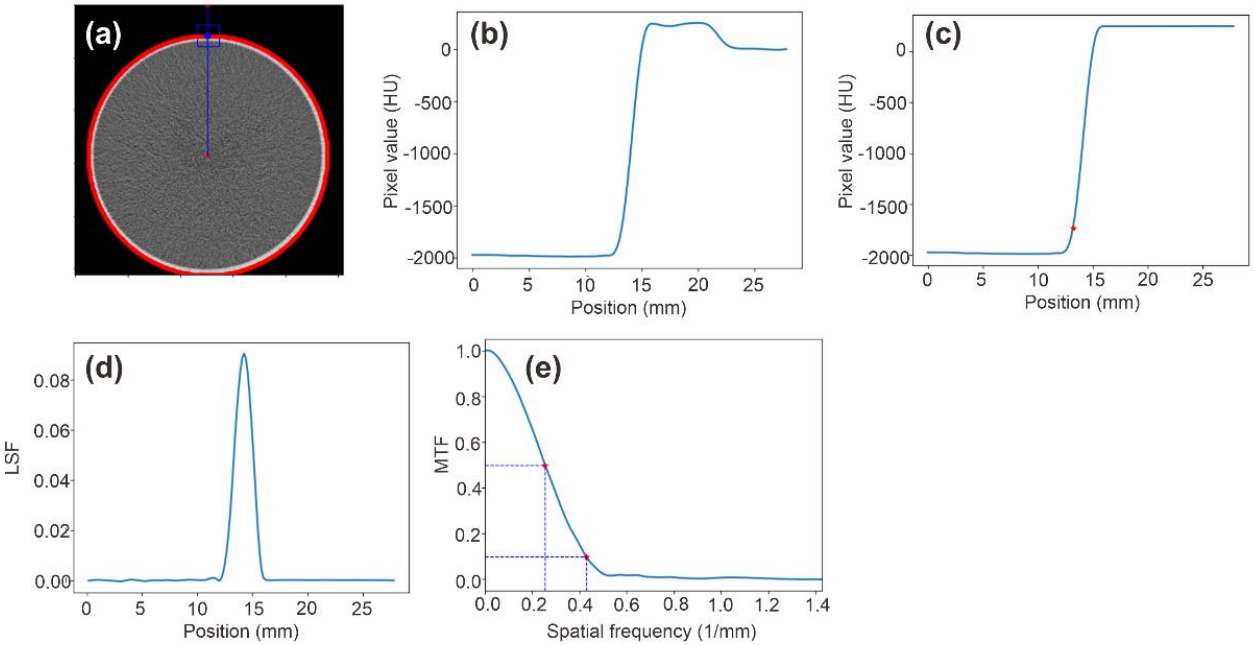

Figure 3. Edge MTF measurement. (**a**) ROI placement on the phantom, (**b**) ESF curve, (**c**) ESF curve after tail replacement, (**d**) LSF curve, and (**e**) MTF curve.

The bilateral filter was applied to these images with the configuration of sigma space (σ_d) = 2, sigma intensity (σ_r) = noise level, and kernel size 5 × 5 pixels. The noise (σ) was obtained using an automatic noise measurement algorithm [38] on the first image. After the images were filtered, the NPS and MTF measurement were performed using the same configuration as before. Filtering was performed repeatedly on the previously filtered image 5 times so that 6 NPS and 6 MTF curves were obtained including the original one. Both NPS and MTF measurement as well as the filtering processes were carried out on 5 slices of a homogeneous water phantom for each variation of tube current to obtain more stable and comprehensive results. Figure 4 shows an example of the filtered images.

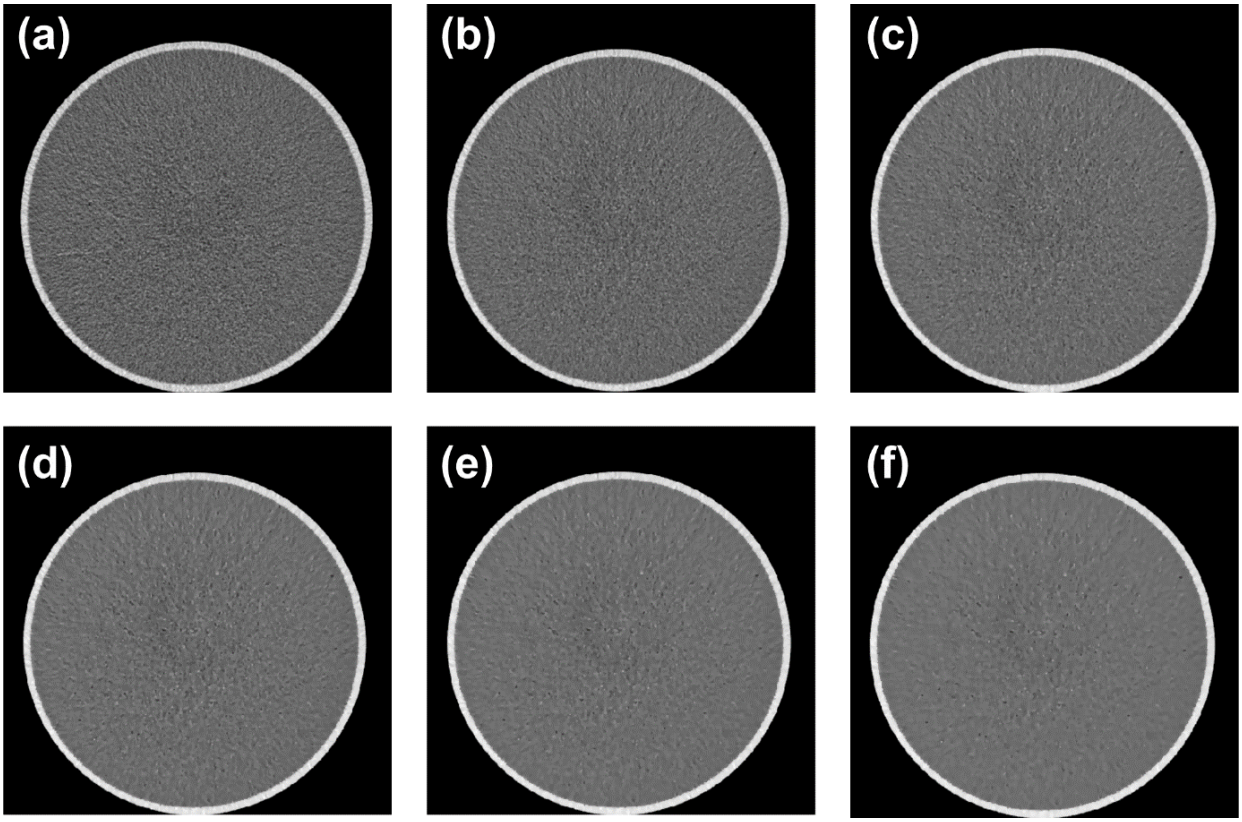

Figure 4. A homogeneous water phantom image on a tube current of 77 mAs filtered repeatedly. (**a**) Original image, filtered image iteratively in (**b**) 1, (**c**) 2, (**d**) 3, (**e**) 4, and (**f**) 5 times.

2.4. Implementation of Anthropomorphic Phantom Images

To observe the impact of bilateral filters in clinical scenarios, we obtained anthropomorphic images with scan parameters as shown in Table 2. As before, the bilateral filter was run for 5 iterations on the head anthropomorphic phantom image. The noise was measured using a circular ROI with a radius of 10 mm in the frontal lobe area (Figure 5a). In terms of spatial resolution, we used visual observations on the visible areas of soft tissue, bone, and air (Figure 5b). Comparisons using structural similarity (SSIM) were also carried out to get a more comprehensive description. SSIM was obtained by comparing the filtered image with the original image.

Table 2. Scan parameters on anthropomorphic phantoms.

Parameter	Value
Scanner	Toshiba Alexion
Tube current (mAs)	100
Tube voltage (kVp)	120
Slice thickness (mm)	7
Scan option	Helical
Pitch	1.5
Convolution kernel	FC13
Image reconstruction	Filtered-back projection

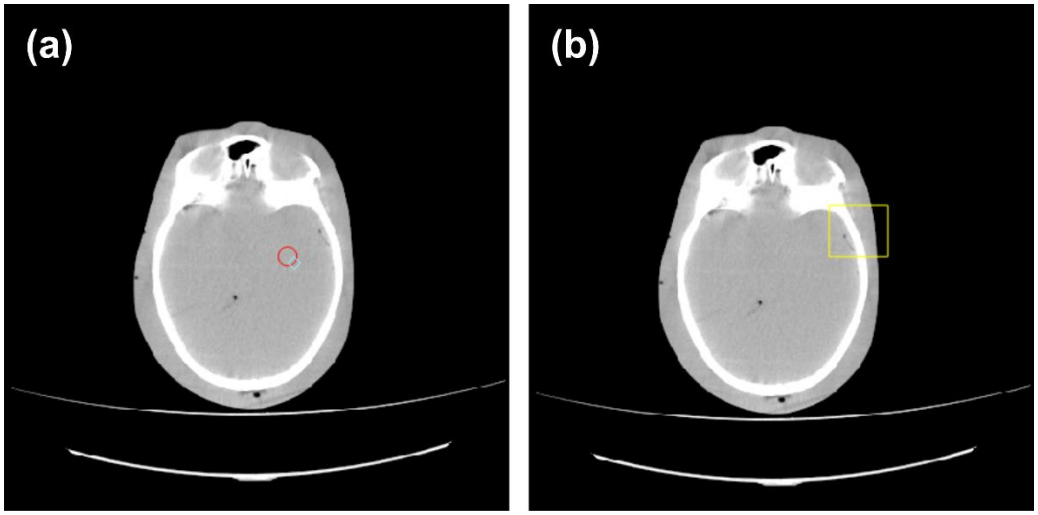

Figure 5. Anthropomorphic phantom image of the head. (**a**) ROI for measuring noise, (**b**) ROI for observing spatial resolution.

3. Results

3.1. Tube Current of 77 mAs

Figure 6 shows the 1D NPS at each filter iteration. The NPS at a frequency of about 0.2 mm^{-1} decreased significantly with the number of filter iterations. The peak frequency is shifted to a lower value, and the NPS at very high frequencies (>0.4 mm^{-1}) was almost completely suppressed by the 5th iteration. This shows the effectiveness of the bilateral filter in filtering noise at high frequencies.

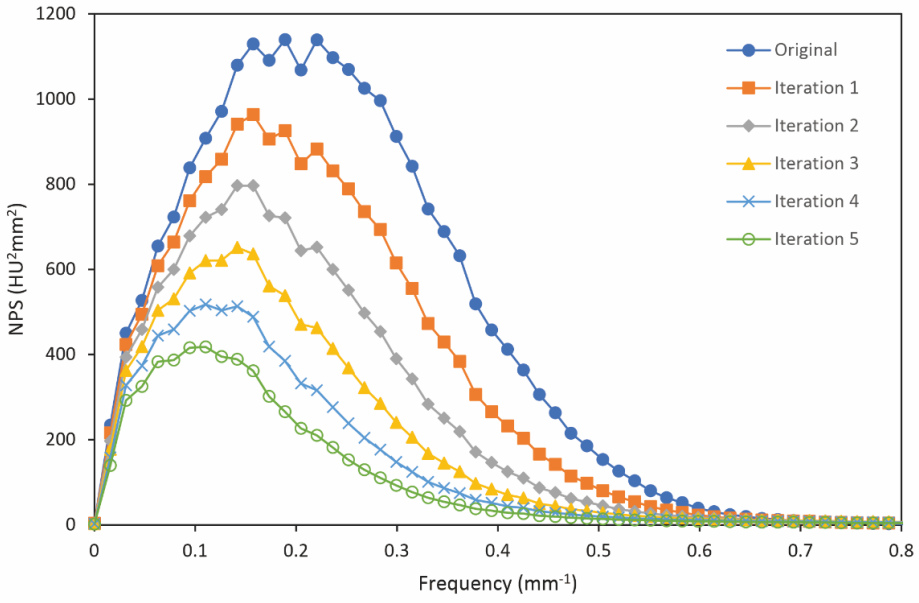

Figure 6. NPS on repeatedly filtered images at a tube current of 77 mAs.

Figure 7 shows the noise of the original image and the filtered image in five iterations with a tube current of 77 mAs. The noise magnitude decreased while the percentage of reduced noise increased with the number of filter iterations. The peak frequency and mean frequency shifted down gradually from 0.19 mm^{-1} to 0.11 mm^{-1} and from 0.24 mm^{-1} to 0.17 mm^{-1}, respectively. These results indicate a decrease in NPS at a certain frequency as a result of repeated filtering at low tube currents.

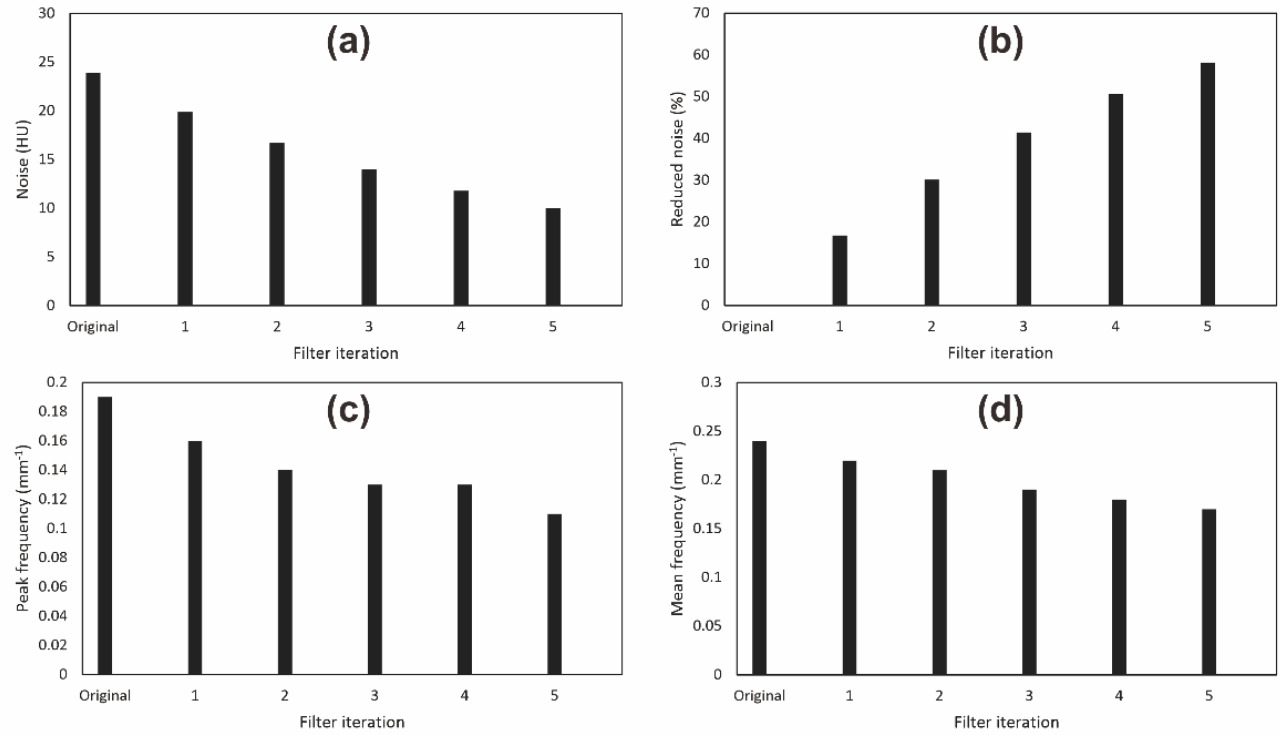

Figure 7. Noise measurement on homogeneous phantom with tube current of 77 mAs. (**a**) Noise, (**b**) Percentage of reduced noise, (**c**) Peak frequency, and (**d**) Mean frequency.

Figure 8 shows the spatial resolution of each filter iteration at a tube current of 77 mAs. Table 3 shows the MTF50 and MTF10 values. MTF curves that coincide after each filter iteration indicate that no degradation of the spatial resolution of the image due to iteration. This was also confirmed by the MTF50 and MTF10 values which did not change significantly. This shows the ability of bilateral filters to maintain the spatial resolution of the image.

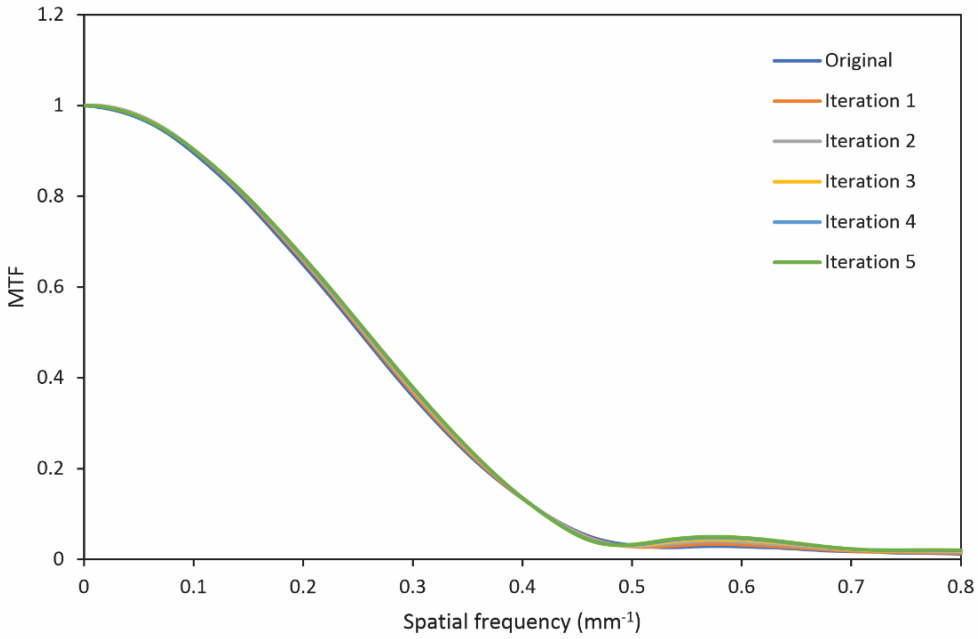

Figure 8. The MTF curve obtained from the edge of the image in 5 filter iterations at a tube current of 77 mAs.

Table 3. MTF50 and MTF10 value for every filter iteration at tube current of 77 mAs.

Filter Iteration	MTF50 (mm^{-1})	MTF10 (mm^{-1})
Original	0.25	0.42
1	0.25	0.42
2	0.26	0.42
3	0.26	0.42
4	0.26	0.42
5	0.26	0.42

3.2. Tube Current of 154 mAs

Figure 9 shows the impact of iterative filtration on an image using a tube current of 154 mAs. With increasing filter iterations, the noise at frequencies around >0.2 mm^{-1} decreases considerably, flattening the tail of the NPS curve

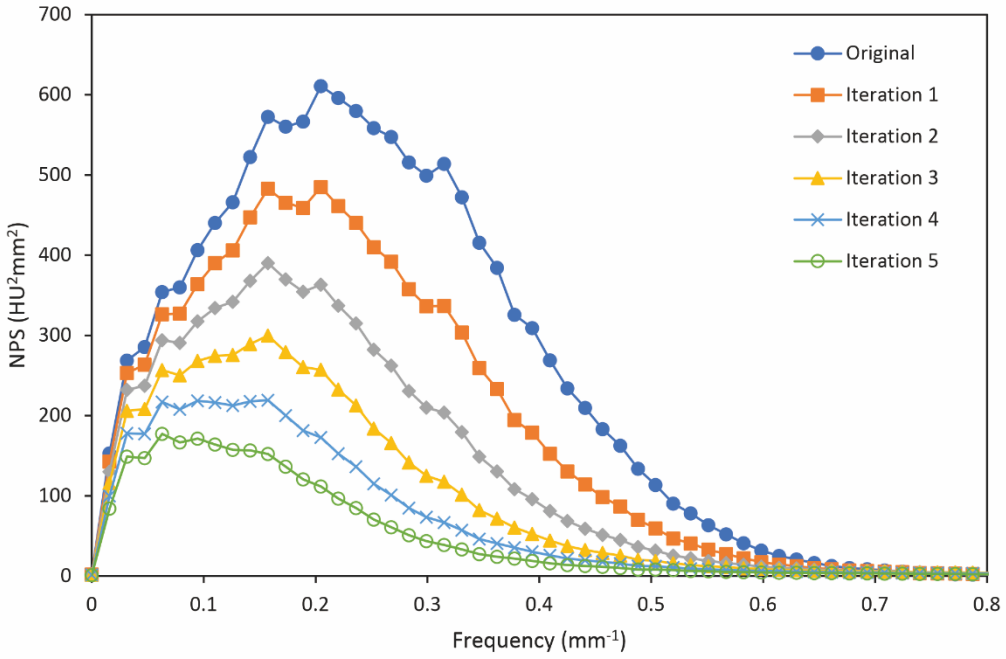

Figure 9. NPS on repeated filtered images at a tube current of 154 mAs.

Figure 10 shows the noise of the original image and the filtered image with up to five iterations at tube current 154 mAs. The noise was reduced by more than half of its original values. The peak frequency gradually shifted from 0.2 to 0.09 mm^{-1} after five iterations, and the mean frequency decreased from 0.25 to 0.18 mm^{-1}.

Figure 11 shows the spatial resolution of each filter iteration at a tube current of 154 mAs. Table 4 shows the MTF50 and MTF10 values. Similar to Figure 8, the MTF curves coincide with each other, indicating no change in spatial resolution for each filter iteration. The MTF values shown in Table 4 also do not show any change.

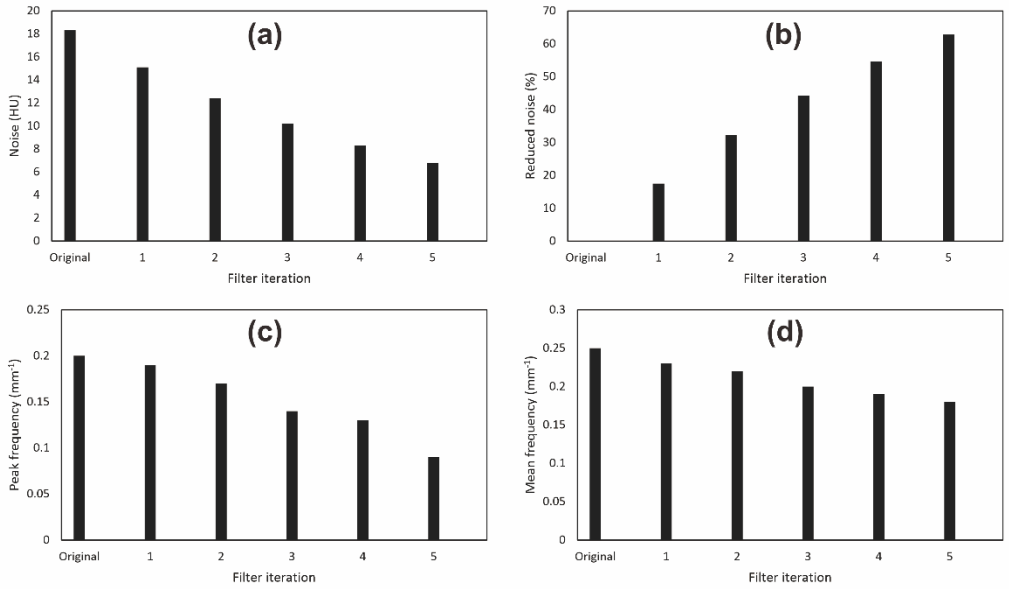

Figure 10. Noise measurement on homogeneous phantom with tube current of 154 mAs. (**a**) Noise, (**b**) Percentage of reduced noise, (**c**) Peak frequency, and (**d**) Mean frequency.

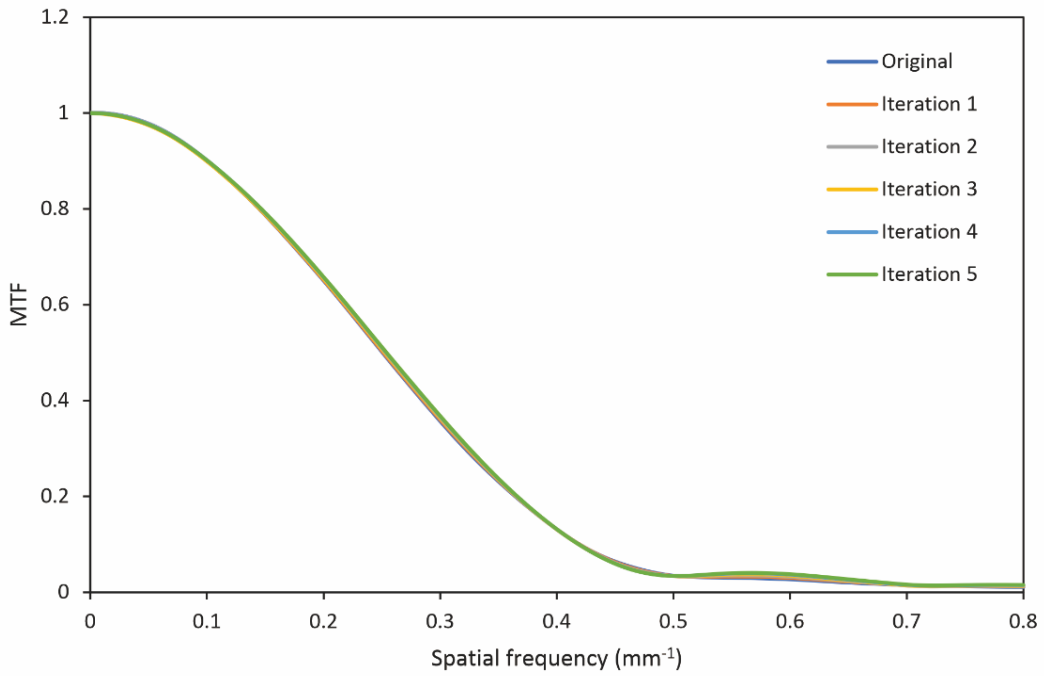

Figure 11. The MTF curve obtained from the edge of the image in 5 filter iterations at a tube current of 154 mAs.

Table 4. MTF50 and MTF10 value for every filter iteration at tube current of 154 mAs.

Filter Iteration	MTF50 (mm^{-1})	MTF10 (mm^{-1})
Original	0.25	0.42
1	0.25	0.42
2	0.25	0.42
3	0.25	0.42
4	0.25	0.42
5	0.25	0.42

3.3. Tube Current of 231 mAs

Figure 12 shows the impact of iterative filtration on an image using a tube current of 231 mAs. In the original image, the noise peaks at a frequency of about 0.2 mm^{-1}. By filtering it for many iterations, the noise at high frequencies gradually decreased, leaving more at a low frequency.

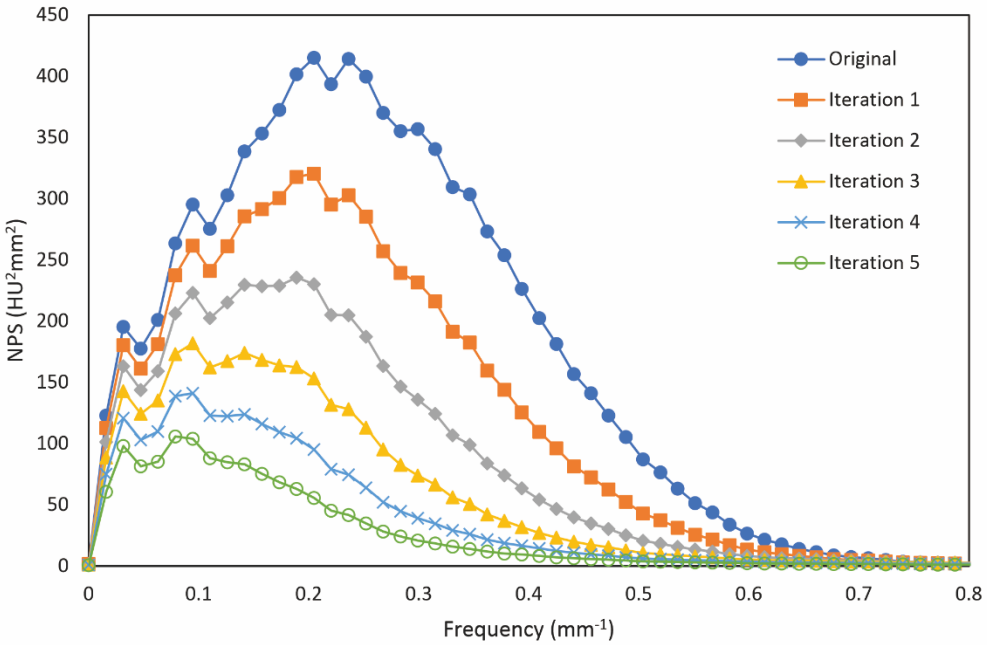

Figure 12. NPS on repeated filtered images at tube current of 231 mAs.

Figure 13 shows the NPS characteristics of the original image and the filtered image at up to five iterations for at tube current of 231 mAs. For five iterations of filtration, the noise magnitude decreased by more than 60%. The peak frequency dramatically shifted from 0.22 to 0.06 mm^{-1} and the average frequency gradually decreased from 0.26 to 0.17 mm^{-1}.

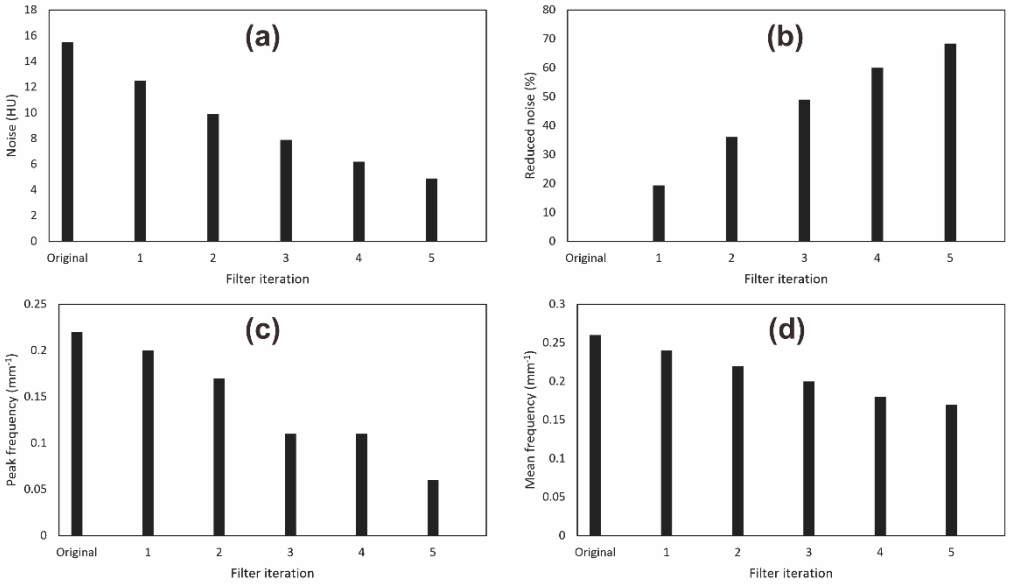

Figure 13. Noise measurement on homogeneous phantom with tube current of 231 mAs. (**a**) Noise, (**b**) Percentage of reduced noise, (**c**) Peak frequency, and (**d**) Mean frequency.

Figure 14 shows the spatial resolution of each filter iteration at a tube current of 154 mAs. Table 5 shows the MTF50 and MTF10 values for a tube current of 231 mAs. In Figure 14, the MTF curves coincide, indicating that iterative bilateral filtering leads to no change in spatial resolution. The MTF values shown in Table 5 also do not show any change for a tube current of 231 mAs, identical to a tube current of 154 mAs (Table 4).

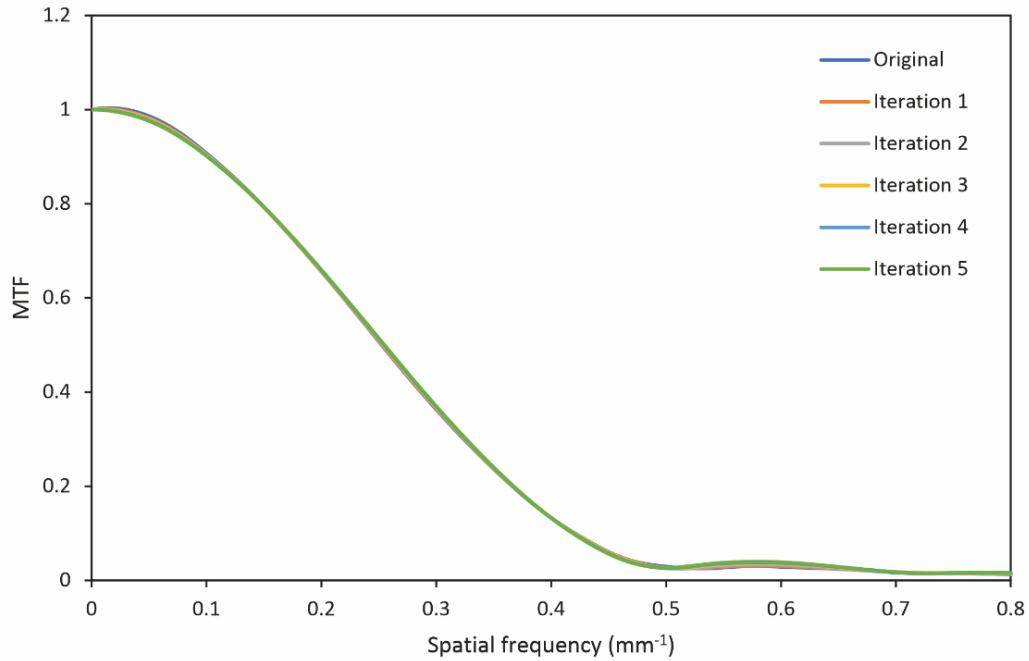

Figure 14. The MTF curve obtained from the edge of the image in 5 filter iterations at a tube current of 231 mAs.

Table 5. MTF50 and MTF10 value for every filter iteration at tube current of 231 mAs.

Filter Iteration	MTF50 (mm^{-1})	MTF10 (mm^{-1})
Original	0.25	0.42
1	0.25	0.42
2	0.25	0.42
3	0.25	0.42
4	0.25	0.42
5	0.25	0.42

3.4. Impact of Bilateral Filter on Anthropomorphic Images

Figure 15 shows noise measurements in the five iterations of the bilateral filter in the frontal lobe. It can be seen that, in the frontal lobe area, the bilateral filter can reduce noise by more than 60%, showing its effectiveness in reducing noise gradually as the filter iterations. The effects on spatial resolution can be seen in Figure 16. The bilateral filters did not significantly alter the structure at the edge between bone and soft tissue. There were no blurred edges or distortions at the edges between networks. Likewise, at the edge of the phantom with air, no significant changes were observed. This shows that the bilateral filter can maintain the edges of the object well, even though it is iterated many times. However, the soft tissue region looks more unnatural in the fifth iteration. These results are characterized using the SSIM presented in Table 6. SSIM decreases with filter iteration, but is never less than 0.5. This decrease is due to effective noise reduction and results in differences in the overall texture of the image.

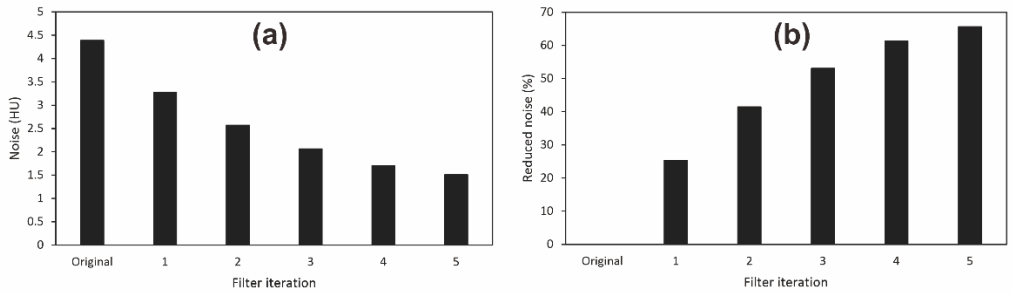

Figure 15. Measurement of noise in the head anthropomorphic phantom image. (**a**) Noise level, (**b**) percentage of reduced noise.

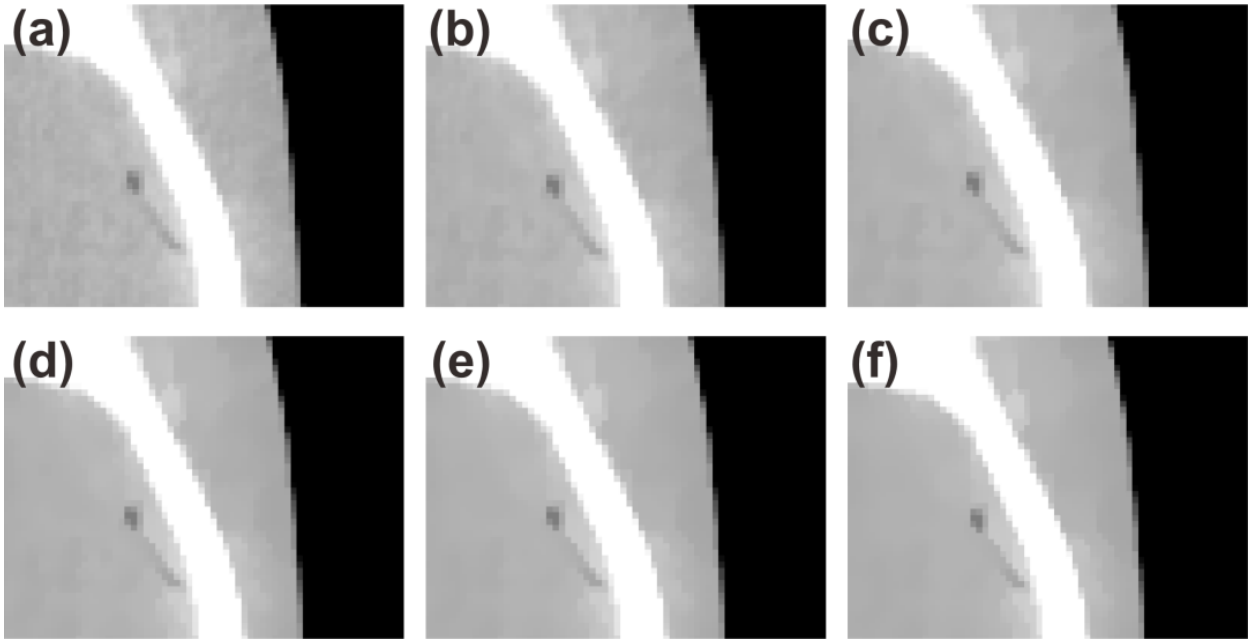

Figure 16. Anthropomorphic phantom images were filtered using a bilateral filter. (**a**) Original image, filtered image in (**b**) 1, (**c**) 2, (**d**) 3, (**e**) 4, and (**f**) 5 times iterations.

Table 6. Similarity index (SSIM) for each filter iteration.

Filter Iteration	SSIM
1	0.85
2	0.69
3	0.60
4	0.54
5	0.50

4. Discussion

This study aims to describe the characteristics of bilateral filters in filtering noise at various frequencies and their patterns in iterative filtering. We used the 1D NPS to characterize image noise. Previous studies that have been carried out have only explored the implementation of bilateral filters without iteration [21,32,39].

Bilateral filters increasingly suppress noise with each iteration. Figure 7, Figure 10, and Figure 13 show that with five iterations, the bilateral filter can suppress noise by more than 50%. This was observed in a homogeneous image with a homogeneous distribution of noise. Observations on areas with objects of various attenuations still need to be evaluated in the future. Anam et al. (2020) investigated several filter algorithms, including bilateral filters, using an in-house point phantom. Their results showed that bilateral filters can

reduce noise by up to 18% for a single filter iteration, compared to the adaptive mean filter (AMF) which reduced noise by up to 29%, and the selective mean filter (SMF) which reduced it by up to 27%. The bilateral filter is not as aggressive as these other filters in reducing noise, but it maintains better spatial resolution [9].

Apart from the reduced noise magnitude, the texture also changes. The data showed interesting properties of bilateral filters in changing the noise texture. In the original images with tube currents of 77, 154, and 231 mAs, the NPS showed the peak frequency was about 0.2 mm^{-1}. When the images were filtered five times, the peak frequency shifted to lower values (Figures 6, 9 and 12). This phenomenon shows that the bilateral filter suppresses noise at high frequencies more aggressively than noise at low frequencies. By the fifth iteration, the NPS curve showed a flattening of its shape at frequencies above 0.2 mm^{-1}.

The loss of high-frequency noise caused the bilateral filters to suppress soft (i.e., smooth) textures. In an image with visible gradation, this behavior will give the appearance of a staircase effect, and make the image less realistic. There are several extensions and variants of the bilateral filter that have been developed to deal with this effect [13,40]. Notwithstanding, the bilateral filter shows very good results in reducing noise in general, especially in maintaining object edges when compared to other linear filters such as the mean filters and Gaussian filters. This was confirmed by the MTF50 and MTF10 obtained from the phantom edge which did not change significantly with filter iteration for all tube currents (Tables 3–5). This is an advantage of bilateral filters in clinical practice, where most filter algorithms tend to limit the spatial resolution to be able to suppress the noise. This was verified by testing the anthropomorphic phantom images. Behavior similar to that with the homogeneous phantom was observed, with noise decreasing with filter iteration (Figure 15). In the fifth iteration, noise is reduced by more than 60% (i.e., from 4.39 to 1.51 HU) in the frontal lobe area. In addition, the bilateral filter did not show aggressive behavior towards the edges of objects. In Figure 16, the edge between bone and soft tissue still looks sharp until the fifth iteration. There are no blurred edges or reverse effects. However, an unnatural appearance can be observed in the homogeneous areas of soft tissue. This causes the SSIM to decrease with increasing filter iterations. However, even with five iterations, the similarity does not fall below 0.5.

Knowledge of the noise texture becomes important in determining the most suitable strategy in the denoising procedure because each filter has different characteristics and must be adapted to the type of noise and the clinical purpose [41]. In the case of the bilateral filter, the configuration is more efficient if it is set according to the noise level. Small values of sigma intensity (σ_r) will make the edges of an object look sharper, while a higher value will make it behave more like a Gaussian filter which reduces more noise but blurs the edges [32]. A study by Peng (2010) [21] recommended $\sigma_r = 2.5\,\sigma$ for the best results on artificial images with Gaussian noise based on the peak signal-to-ratio (PSNR) value. In the case of medical images, further investigations need to be carried out to determine the optimal parameters for diagnostic purposes.

This study observes the iterative effect of bilateral filters on homogeneous and anthropomorphic phantom images and was not implemented on patient images. This study is the first step in investigating the effect of the bilateral filter on noise texture. Our findings are relevant only within the scope of the QA procedure. Investigations of patient images will be performed in future studies by an expert radiologist.

The paper only investigates the iterative bilateral filter in improving CT images; however, this approach can be implemented on other images such as images from mammography, magnetic resonance imaging (MRI), ultrasound (US), and other sources.

In addition to bilateral filters, state-of-the-art filters such as the non-local mean filter (NLM) [42] are also interesting to explore in terms of changing the image structure with increasing iterations. Since iterative reconstruction (IR) [43] and deep learning reconstruction (DLR) [44] produce non-linear properties in terms of noise and spatial resolution, it would be interesting to examine the impact of the NLM filter on IR and DLR images and to compare it with the bilateral filter.

5. Conclusions

The impact of bilateral filters in changing the noise texture and spatial resolution in CT images has been characterized. After five iterations, the bilateral filter shows its effectiveness in filtering noise at high frequencies as indicated by the flattening of the NPS curve on images produced with tube currents of 77, 154, and 231 mAs. The peak frequency shifts from about 0.2 to about 0.1 mm^{-1} for these tube currents and the noise magnitude was reduced by more than 50%. The spatial resolution does not change with increasing iterations of the filter, which is confirmed by the constant values of MTF50 and MTF10. The test results on an anthropomorphic phantom image show a similar pattern, with noise reduced by up to 60% and object edges remaining sharp. The impact of bilateral filters on clinical images and CT raw data still needs to be investigated in further studies.

Author Contributions: Conceptualization, C.A.; methodology, C.A. and H.S.; software, C.A., A.N. and K.A.; writing, C.A., A.N. and G.D. All authors have read and agreed to the published version of the manuscript.

Funding: This work was funded by the Riset Publikasi International Bereputasi Tinggi (RPIBT), Diponegoro University, No. 569-187/UN7.D2/PP/VII/2022.

Data Availability Statement: Not applicable.

Conflicts of Interest: The authors declare no conflict of interest.

References

1. Pearce, M.S.; Salotti, J.A.; Little, M.P.; McHugh, K.; Lee, C.; Kim, K.P.; Howe, N.L.; Ronckers, C.M.; Rajaraman, P.; Craft, A.W. Radiation exposure from CT scans in childhood and subsequent risk of leukaemia and brain tumours: A retrospective cohort study. *Lancet* **2012**, *380*, 499–505. [CrossRef]
2. Albert, J.M. Radiation risk from CT: Implications for cancer screening. *Am. J. Roentgenol.* **2013**, *201*, W81–W87. [CrossRef] [PubMed]
3. Chen, J.X.; Kachniarz, B.; Gilani, S.; Shin, J.J. Risk of malignancy associated with head and neck CT in children: A systematic review. *Otolaryngol.–Head Neck Surg.* **2014**, *151*, 554–566. [CrossRef] [PubMed]
4. Yeung, A.W.K. The "As Low As Reasonably Achievable" (ALARA) principle: A brief historical overview and a bibliometric analysis of the most cited publications. *Radioprotection* **2019**, *54*, 103–109. [CrossRef]
5. Ning, P.; Zhu, S.; Shi, D.; Guo, Y.; Sun, M. X-ray dose reduction in abdominal computed tomography using advanced iterative reconstruction algorithms. *PLoS ONE* **2014**, *9*, e92568. [CrossRef] [PubMed]
6. Barreto, I.; Verma, N.; Quails, N.; Olguin, C.; Correa, N.; Mohammed, T.L. Patient size matters: Effect of tube current modulation on size-specific dose estimates (SSDE) and image quality in low-dose lung cancer screening CT. *J. Appl. Clin. Med. Phys.* **2020**, *21*, 87–94. [CrossRef]
7. Whitebird, R.R.; Solberg, L.I.; Bergdall, A.R.; López-Solano, N.; Smith-Bindman, R. Barriers to CT Dose Optimization: The Challenge of Organizational Change. *Acad. Radiol.* **2021**, *28*, 387–392. [CrossRef]
8. Li, Z.; Yu, L.; Trzasko, J.D.; Lake, D.S.; Blezek, D.J.; Fletcher, J.G.; McCollough, C.H.; Manduca, A. Adaptive nonlocal means filtering based on local noise level for CT denoising. *Med. Phys.* **2014**, *41*, 011908. [CrossRef]
9. Anam, C.; Adi, K.; Sutanto, H.; Arifin, Z.; Budi, W.S.; Fujibuchi, T.; Dougherty, G. Noise reduction in CT images using a selective mean filter. *J. Biomed. Phys. Eng.* **2020**, *10*, 623–634. [CrossRef]
10. Cropp, R.J.; Seslija, P.; Tso, D.; Thakur, Y. Scanner and kVp dependence of measured CT numbers in the ACR CT phantom. *J. Appl. Clin. Med. Phys.* **2013**, *14*, 338–349. [CrossRef]
11. Einstein, S.A.; Rong, X.J.; Jensen, C.T.; Liu, X. Quantification and homogenization of image noise between two CT scanner models. *J. Appl. Clin. Med. Phys.* **2020**, *21*, 174–178. [CrossRef] [PubMed]
12. Takenaga, T.; Katsuragawa, S.; Goto, M.; Hatemura, M.; Uchiyama, Y.; Shiraishi, J. Modulation transfer function measurement of CT images by use of a circular edge method with a logistic curve-fitting technique. *Radiol. Phys. Technol.* **2015**, *8*, 53–59. [CrossRef] [PubMed]
13. Wang, J. Construction of local nonlinear filter without staircase effect in image restoration. *Appl. Anal.* **2011**, *90*, 1257–1273. [CrossRef]
14. Masoomi, M.A.; Al-Shammeri, I.; Kalafallah, K.; Elrahman, H.M.; Ragab, O.; Ahmed, E.; Al-Shammeri, J.; Arafat, S. Wiener filter improves diagnostic accuracy of CAD SPECT images-comparison to angiography and CT angiography. *Medicine* **2019**, *98*, e14207. [CrossRef] [PubMed]
15. Vasilache, S.; Ward, K.; Cockrell, C.; Ha, J.; Najarian, K. Unified wavelet and Gaussian filtering for segmentation of CT images; application in segmentation of bone in pelvic CT images. *BMC Med. Inform. Decis. Mak.* **2009**, *9* (Suppl. 1), S8. [CrossRef]

16. Patil, P.D.; Kumbhar, A.D. Bilateral Filter for Image Denoising. In Proceedings of the 2015 International Conference on Green Computing and Internet of Things (ICGCIoT), Greater Noida, India, 8–10 October 2015; pp. 299–302.
17. Zhang, M.; Gunturk, B.K. Multiresolution bilateral filtering for image denoising. *IEEE Trans. Image Process.* **2008**, *17*, 2324–2333. [CrossRef]
18. Zhang, B.; Allebach, J.P. Adaptive bilateral filter for sharpness enhancement and noise removal. *IEEE Trans. Image Process.* **2008**, *17*, 664–678. [CrossRef]
19. Joseph, J.; Periyasami, R. An image driven bilateral filter with adaptive range and spatial parameters for denoising Magnetic Resonance Images. *Comput. Electr. Eng.* **2018**, *6*, 782–795. [CrossRef]
20. Zheng, Y.; Fu, H.; Au, O.K.-C.; Tai, C.-L. Bilateral Normal Filtering for Mesh Denoising. *IEEE Trans. Vis. Comput. Graph.* **2011**, *17*, 1521–1530. [CrossRef]
21. Peng, H.; Rao, R. Bilateral kernel parameter optimization by risk minimization. In Proceedings of the IEEE International Conference on Image Processing, Hong Kong, China, 26–29 September 2010; pp. 3293–3296.
22. Akar, S.A. Determination of optimal parameters for bilateral filter in brain MR image denoising. *Appl. Soft Comput.* **2016**, *43*, 87–96. [CrossRef]
23. Ghosh, S.; Nair, P.; Chaundhury, K.N. Optimized Fourier Bilateral Filtering. *IEEE Signal Process. Lett.* **2018**, *25*, 1555–1559. [CrossRef]
24. Xu, H.; Zhang, Z.; Gao, Y.; Liu, H.; Xie, F.; Li, J. Adaptive Bilateral Texture Filter for Image Smoothing. *Front. Neurorobot.* **2022**, *16*, 729924. [CrossRef] [PubMed]
25. Bronstein, M.M. Lazy Sliding Window Implementation of the Bilateral Filter on Parallel Architectures. *IEEE Trans. Image Process.* **2011**, *20*, 1751–1756. [CrossRef]
26. Galiano, G.; Velasco, J. On a Fast Bilateral Filtering Formulation Using Functional Rearrangements. *J. Math. Imaging Vis.* **2015**, *53*, 346–363. [CrossRef]
27. Paris, S.; Kornprobst, P.; Tumblin, J.; Durand, F. Bilateral Filtering: Theory and Applications. *Found. Trends Comput. Graph. Vis.* **2009**, *4*, 1–73. [CrossRef]
28. Anh, D.N. Iterative Bilateral Filter and Non-Local Mean. *Int. J. Comput. Appl.* **2014**, *106*, 33–38.
29. Zeng, R.; Gavrielides, M.A.; Petrick, N.; Sahiner, B.; Li, Q.; Myers, K.J. Estimating local noise power spectrum from a few FBP-reconstructed CT scans. *Med. Phys.* **2016**, *43*, 568–582. [CrossRef]
30. Li, G.; Liu, X.; Dodge, C.T.; Jensen, C.T.; Rong, X.J. A noise power spectrum study of a new model-based iterative reconstruction system: Veo 3.0. *J. Appl. Clin. Med. Phys.* **2016**, *17*, 428–439. [CrossRef]
31. Dolly, S.; Chen, H.C.; Anastasio, M.; Mutic, S.; Li, H. Practical considerations for noise power spectra estimation for clinical CT scanners. *J. Appl. Clin. Med. Phys.* **2016**, *17*, 392–407. [CrossRef]
32. Park, J.; Han, J.; Lee, B. Performance of bilateral filtering on Gaussian noise. *J. Electron. Imag.* **2014**, *23*, 043024. [CrossRef]
33. Solomon, J.B.; Christianson, O.; Samei, E. Quantitative comparison of noise texture across CT scanners from different manufacturers. *Med. Phys.* **2012**, *39*, 6048–6055. [CrossRef] [PubMed]
34. Samei, E.; Bakalyar, D.; Boedeker, K.L.; Brady, S.; Fan, J.; Leng, S.; Myers, K.J.; Popescu, L.M.; Ramirez Giraldo, J.C.; Ranallo, F.; et al. Performance evaluation of computed tomography systems: Summary of AAPM Task Group 233. *Med. Phys.* **2019**, *46*, e735–e756. [CrossRef]
35. ImQuest. Available online: https://deckard.duhs.duke.edu/~{}samei/tg233.html (accessed on 10 July 2022).
36. Anam, C.; Budi, W.S.; Fujibuchi, T.; Haryanto, F.; Dougherty, G. Validation of the tail replacement method in MTF calculations using the homogeneous and non-homogeneous edges of a phantom. *J. Phys. Conf. Ser.* **2019**, *1248*, 012001. [CrossRef]
37. Anam, C.; Naufal, A.; Fujibuchi, T.; Matsubara, K.; Dougherty, G. Automated development of the contrast-detail curve based on statistical low-contrast detectability in CT images. *J. Appl. Clin. Med. Phys.* **2022**, *9*, e13719. [CrossRef]
38. Anam, C.; Arif, I.; Haryanto, F.; Lestari, F.P.; Widita, R.; Budi, W.S.; Sutanto, H.; Adi, K.; Fujibuchi, T.; Dougherty, G. An improved method of automated noise measurement system in CT images. *J. Biomed. Phys. Eng.* **2021**, *11*, 163–174. [PubMed]
39. Mendrik, A.M.; Vonken, E.J.; van Ginneken, B.; de Jong, H.W.; Riordan, A.; van Seeters, T.; Smit, E.J.; Viergever, M.A.; Prokop, M. TIPS bilateral noise reduction in 4D CT perfusion scans produces high-quality cerebral blood flow maps. *Phys. Med. Biol.* **2011**, *56*, 3857–3872. [CrossRef] [PubMed]
40. Buades, A.; Coll, B.; Morel, J.M. The staircasing effect in neighborhood filters and its solution. *IEEE Trans. Image Process.* **2006**, *15*, 1499–1505. [CrossRef] [PubMed]
41. Al-Hinnawi, A.R.; Daear, M.; Huwaijah, S. Assessment of bilateral filter on 1/2-dose chest-pelvis CT views. *Radiol. Phys. Technol.* **2013**, *6*, 385–398. [CrossRef] [PubMed]
42. Buades, A.; Coll, B.; Morel, J.M. A non-local algorithm for image denoising. In Proceedings of the IEEE Computer Society Conference on Computer Vision and Pattern Recognition (CVPR'05), San Diego, CA, USA, 20–25 June 2005; Volume 2, pp. 60–65.
43. Stiller, W. Basics of iterative reconstruction methods in computed tomography: A vendor-independent overview. *Eur. J. Radiol.* **2018**, *109*, 147–154. [CrossRef]
44. McLeavy, C.M.; Chunara, M.H.; Gravell, R.J.; Rauf, A.; Cushnie, A.; Talbot, C.S.; Hawkins, R.M. The future of CT: Deep learning reconstruction. *Clin. Radiol.* **2021**, *76*, 407–415. [CrossRef]